Optim Eng (2007) 8: 341–372
DOI 10.1007/s11081-007-9003-5

Application of a sensitivity equation method to the k–ϵ model of turbulence

É. Turgeon · D. Pelletier · J. Borggaard · S. Etienne

Received: 19 February 2004 / Revised: 10 August 2006 /
Published online: 17 May 2007

Abstract In this paper, we present some examples of sensitivity analysis for flows modeled by the standard k–ϵ model of turbulence with wall functions. The flow and continuous sensitivity equations are solved using an adaptive finite element method. Our examples emphasize a number of applications of sensitivity analysis: identification of the most significant parameters, analysis of the flow model, assessing the influence of closure coefficients, calculation of nearby flows, and uncertainty analysis. The sensitivity parameters considered are closure coefficients of the turbulence model and constants appearing in the wall functions.

Keywords Sensitivity equation method · k–ϵ model · Reynolds-averaged Navier–Stokes equations · Adaptive mesh · Finite element method · Uncertaintly · Fast nearby flows

Abbreviations

SEM	Sensitivity Equation Method
RANS	Reynolds-Averaged Navier–Stokes Equations

Variables

a	Design parameter
$C_1, C_2, C_\mu, \sigma_k, \sigma_\epsilon$	k–ϵ model constants
C_f	Skin friction coefficient
d	Imposed distance to the wall

É. Turgeon · D. Pelletier (✉) · S. Etienne
Département de Génie Mécanique, École Polytechnique de Montréal, Montréal, PQ, H3C 3A7, Canada
e-mail: dominique.pelletier@polymtl.ca

J. Borggaard
Interdisciplinary Center for Applied Mathematics, Department of Mathematics, Virginia Tech, Blacksburg, VA 24061-0531, USA

E	Roughness parameter
k	Turbulent kinetic energy
$\mathcal{K}$	Natural logarithm of k
L	Reference length
p	Pressure
P	Production of turbulence
Re	Reynolds number
s_x	Sensitivity of the variable x
$\boldsymbol{u}$	Velocity
u, v	Velocity components
u_k	Velocity scale based on k
u_{**}	Friction velocity $\tau_w = \rho u_{**} u_k$
x, y	Cartesian coordinates
y	Distance to the wall
ϵ	Turbulent dissipation rate
$\mathcal{E}$	Natural logarithm of ϵ
κ	Kármán constant
μ	Viscosity
μ_t	Eddy viscosity
ρ	Density
τ_w	Wall shear stress

Subscripts

t	Tangent to the wall

Superscripts

$'$	Sensitivity (derivative)
$+$	Dimensionless (wall functions)
T	Transpose

1 Introduction

Many efficient flow optimization algorithms use information about the gradient of the cost function. This often leads to calculating flow sensitivities, i.e. derivatives of the flow variables with respect to the design parameters. This is known as sensitivity analysis. When the number of design parameters is large, adjoint techniques offer a clear advantage over sensitivity-based techniques (Gunzburger 1999). However, adjoint techniques are specifically developed for optimization problems, whereas sensitivities are defined independently of an optimization problem and may be used for a variety of other applications such as:

- identification of key parameters controlling the flow (Blackwell et al. 1998) (the important parameters),
- identification of parameters that have little effect (Blackwell et al. 1998) (the negligible parameters),
- fast evaluation of solution for nearby values of the parameters (Godfrey et al. 1998),

- the fast evaluation of rate derivatives (Limache and Cliff 1999),
- uncertainty analysis (Blackwell et al. 1998; Turgeon et al. 2001b).

Such applications have been presented by the authors for laminar flows (Turgeon et al. 2000a, 2000b, 2000c, 2001a, 2001b; Borggaard et al. 2000) and by Godfrey and Cliff (2001) for compressible turbulent flows. In Godfrey and Cliff (2001) the focus is on external compressible turbulent flow while the present work is on incompressible turbulent flows (external and internal). Furthermore, the present work uses a general sensitivity equation method while Godfrey and Cliff treat a more restricted class of SEM in which portions of the turbulence model are not differentiated with respect to the parameter. In the present work, all terms in the turbulence model are differentiated through the implicit function theorem. The present SEM is thus complete and thoroughly consistent with the flow equations. In this paper, a number of applications are studied for turbulent incompressible flows (using the k–ϵ turbulence model with wall functions).

Our applications focus on the closure coefficients and the parameters appearing in wall functions. We have selected these for two reasons. First, they constitute a good example of how sensitivity analysis can be used in the context of turbulence modeling. Indeed, sensitivities provide a richer base of information on which a modeler can rely for interpreting his simulation data. Secondly, these parameter fall in the category of value parameters which do not affect the geometry of the computational domain. Shape parameters are beyond the scope of this paper due to the special computational challenges. These difficulties are briefly discussed in the paper.

In the next section, we discuss the flow equations and boundary conditions. We then present an example of the continuous sensitivity equations and their boundary conditions. A previous paper (Turgeon et al. 2004) provides more detail about the general formulation and its implementation in an adaptive finite element solver. In this paper, we emphasize applications rather than the formulation. Three examples are used to illustrate the application of the methodology and different roles of the sensitivities. The first is the decay of grid turbulence. This problem has a closed form solution and is used to verify the code. Sensitivity analysis for flow over a backward facing step and flow over a flat plate are then performed. The paper ends with conclusions.

2 Flow equations

2.1 Reynolds-averaged Navier–Stokes equations

The flow regime of interest is modeled by the time-averaged steady-state momentum and continuity equations,

$$\rho \boldsymbol{u} \cdot \nabla \boldsymbol{u} = -\nabla p + \boldsymbol{f} + \nabla \cdot [(\mu + \mu_t)(\nabla \boldsymbol{u} + \nabla \boldsymbol{u}^T)], \tag{1}$$

$$\nabla \cdot \boldsymbol{u} = 0, \tag{2}$$

where ρ is the density, $\boldsymbol{u}$ is the velocity, p is the pressure, and μ is the viscosity, and $\boldsymbol{f}$ is a body force. The eddy viscosity μ_t is computed using the k–ϵ model of

turbulence. Equation (1) incorporates a gradient diffusion model for the Reynolds stresses : $-\rho\overline{u_i' v_j'} = \mu_T[\nabla \boldsymbol{u} + (\nabla \boldsymbol{u})^T]$.

2.2 The standard k–ϵ model of turbulence

The eddy viscosity is expressed in terms of two turbulence variables, the turbulence kinetic energy k and its rate of dissipation ϵ:

$$\mu_t = \rho C_\mu \frac{k^2}{\epsilon}.$$

The mathematical system (1–2) is closed using the standard k–ϵ model of turbulence (Launder and Spalding 1974). To preserve positivity of the dependent variables we work with the logarithmic form of these equations (Ilinca and Pelletier 1998). This can be viewed as using the following change of dependent variables:

$$\mathcal{K} = \ln(k) \quad \text{and} \quad \mathcal{E} = \ln(\epsilon).$$

The transport equations for the logarithmic variables, written in a block-triangular form, are:

$$\begin{aligned}\rho \boldsymbol{u} \cdot \nabla \mathcal{K} = {} & \nabla \cdot \left[\left(\mu + \frac{\mu_t}{\sigma_k}\right)\nabla \mathcal{K}\right] + \left(\mu + \frac{\mu_t}{\sigma_k}\right)\nabla \mathcal{K} \cdot \nabla \mathcal{K} + \mu_t e^{-\mathcal{K}} P \\ & - \rho^2 C_\mu \frac{e^{\mathcal{K}}}{\mu_t} + q_{\mathcal{K}}, \end{aligned} \tag{3}$$

$$\begin{aligned}\rho \boldsymbol{u} \cdot \nabla \mathcal{E} = {} & \nabla \cdot \left[\left(\mu + \frac{\mu_t}{\sigma_\epsilon}\right)\nabla \mathcal{E}\right] + \left(\mu + \frac{\mu_t}{\sigma_\epsilon}\right)\nabla \mathcal{E} \cdot \nabla \mathcal{E} \\ & + \rho C_1 C_\mu e^{\mathcal{K}-\mathcal{E}} P - C_2 \rho e^{\mathcal{E}-\mathcal{K}} + q_{\mathcal{E}}. \end{aligned} \tag{4}$$

In the two equations above, the terms $q_{\mathcal{K}}$ and $q_{\mathcal{E}}$ are user supplied source terms used for code verification (Roache 1998); see the verification example in Sect. 6.1.

The production of turbulence P is defined as

$$P = \nabla \boldsymbol{u}(\nabla \boldsymbol{u} + (\nabla \boldsymbol{u} t)^T).$$

The constants $C_1, C_2, C_\mu, \sigma_k$, and σ_ϵ are set to the values recommended by Launder and Spalding (1974) and given in Table 1.

Note that (3–4) are equivalent to the original equations of the turbulence model; only the computational variables are different. Hence, the turbulence model remains unchanged. In terms of logarithmic variables, the eddy viscosity is now given by

$$\mu_t = \rho C_\mu e^{2\mathcal{K}-\mathcal{E}}.$$

Table 1 Constants for the k–ϵ model

C_μ	C_1	C_2	σ_k	σ_ϵ
0.09	1.44	1.92	1.0	1.3

2.3 Boundary conditions

The flow in the domain Ω is modeled by the Reynolds-averaged Navier–Stokes equations subject to boundary conditions. Typical boundary conditions take the forms:

$$\boldsymbol{u} = \boldsymbol{u}_{bc} \quad \text{on } \Gamma_d \tag{5}$$

for Dirichlet boundary conditions, and

$$-p + \hat{\boldsymbol{n}} \cdot \boldsymbol{\tau}(\boldsymbol{u}) \cdot \hat{\boldsymbol{n}} = 0 \quad \text{and} \quad \boldsymbol{u} \cdot \hat{\boldsymbol{t}} = 0 \quad \text{on } \Gamma_n \tag{6}$$

for outflow conditions, or

$$\boldsymbol{u} \cdot \hat{\boldsymbol{n}} = 0 \quad \text{and} \quad \hat{\boldsymbol{t}} \cdot \boldsymbol{\tau}(\boldsymbol{u}) \cdot \hat{\boldsymbol{n}} = 0 \quad \text{on } \Gamma_s \tag{7}$$

to model symmetry. The stress tensor $\boldsymbol{\tau}(\boldsymbol{u})$ is defined as

$$\boldsymbol{\tau}(\boldsymbol{u}) = (\mu + \mu_t t)(\nabla \boldsymbol{u} + (\nabla \boldsymbol{u} t)^T).$$

Similarly, the boundary conditions on k are

$$k = k_{bc} \quad \text{on } \Gamma_k \tag{8}$$

and

$$\left(\mu + \frac{\mu_t}{\sigma_k}\right) \nabla k \cdot \hat{\boldsymbol{n}} = 0 \quad \text{on } \Gamma_f. \tag{9}$$

A similar form holds for ϵ.

2.4 Wall boundary conditions

The standard k–ϵ turbulence model is not valid when the turbulence Reynolds number is low as is the case near solid walls. The strategy adopted here uses wall functions which describe the solution near the wall. Wall function formulations are offered by most if not all CFD vendors who often recommend them as a first option given their low computational cost compared to low Reynolds number models. Furthermore, wall functions are still the focus of active research (Galera et al. 2005). Hence, they constitute a valid model for sensitivity analysis.

We use a two-velocity scale wall function described in (Chabard 1991; Ignat et al. 1998). The universal velocity profile is given by:

$$u^+ = \begin{cases} y^+ & \text{for } y^+ < y_c^+, \\ \frac{1}{\kappa} \ln(E y^+) & \text{for } y^+ \geq y_c^+ \end{cases} \tag{10}$$

where κ is the Kármán constant and E a roughness parameter. For smooth walls we take $\kappa = 0.42$ and $E = 9.0$. The junction point y_c^+ is obtained from the intersection

of the two curves, in this case $y_c^+ \approx 11$. The dimensionless distance to the wall y^+ and dimensionless tangential velocity u^+ are given by:

$$y^+ = \frac{\rho y u_k}{\mu}, \tag{11}$$

$$u^+ = \frac{u_t}{u_{**}} \tag{12}$$

where u_t is the tangential velocity and y is the normal distance to the wall. These wall functions involve two velocity scales: u_{**}, the friction velocity, and u_k, a velocity scale based on the turbulence kinetic energy and defined as

$$u_k = C_\mu^{1/4} k^{1/2} \tag{13}$$

where k is taken at the boundary of the computational domain.

The corresponding boundary conditions for k, ϵ, and the momentum equations at a distance $y = d$ from the wall are:

$$\frac{\partial k}{\partial n} = 0 \quad \text{or} \quad \left(\mu + \frac{\mu_t}{\sigma_k}\right) \nabla \mathcal{K} \cdot \hat{\boldsymbol{n}} = 0, \tag{14}$$

$$\epsilon = \frac{u_k^3}{\kappa d} \quad \text{or} \quad \mathcal{E} = \ln\left(\frac{u_k^3}{\kappa d}\right), \tag{15}$$

$$\boldsymbol{u} \cdot \hat{\boldsymbol{n}} = 0, \tag{16}$$

$$\tau_w = \rho u_{**} u_k \tag{17}$$

where $\hat{\boldsymbol{n}}$ is the outward normal unit vector. Note that substitution of (10) to (13) into (17) provides a relationship between the wall shear stress τ_w and the velocity u_t, i.e. a mixed or Robin boundary condition.

Of course, the specific value of d where the boundary condition is applied is chosen so that y^+ lies within a safe range of validity of the logarithmic wall function. A posteriori computations of y^+ are always performed to make sure that $30 < y^+ < 300$.

Figure 1 shows typical discretizations of the computational domain close to the wall, for finite elements and finite volumes. In finite elements, the mesh does not reach the wall; wall functions bridge this gap. In finite volumes, a wall function cell is used instead. Its height d must also satisfy $30 < d^+ < 300$. Because the mesh reaches the wall, both u and v are set to zero at the wall. In this case, wall functions determine the values of the velocity at the first nodes off the wall. While simplifying the CFD, meshing to the wall imposes non-trivial constraints on mesh generation to ensure that $30 < d^+ < 300$.

3 Sensitivity equations

3.1 Sensitivity equations for the Reynolds-averaged Navier–Stokes equations

The continuous sensitivity equations (CSE) are derived formally by implicit differentiation of the flow equations (1) and (2) with respect to design parameter a. Thus,

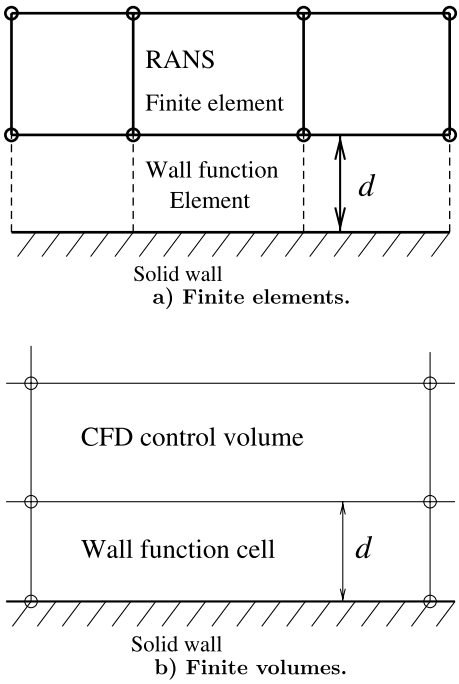

Fig. 1 Discretization close to the wall

not only do we treat the variable $\boldsymbol{u}$ as a function of space, but also as a function of the design parameter a. This dependence is denoted as $\boldsymbol{u}(\boldsymbol{x}; a)$. Defining the flow sensitivities as the partial derivatives $\boldsymbol{s}_u = \frac{\partial \boldsymbol{u}}{\partial a}$ and $s_p = \frac{\partial p}{\partial a}$, and the derivatives of the fluid properties and other flow parameters by a $(')$, we obtain

$$\begin{aligned}
&\rho' \boldsymbol{u} \cdot \nabla \boldsymbol{u} + \rho \boldsymbol{s}_u \cdot \nabla \boldsymbol{u} + \rho \boldsymbol{u} \cdot \nabla \boldsymbol{s}_u \\
&\quad = -\nabla s_p + \boldsymbol{f}' + \nabla \cdot [(\mu' + \mu_t')(\nabla \boldsymbol{u} + (\nabla \boldsymbol{u})^T) + (\mu + \mu_t)(\nabla \boldsymbol{s}_u + (\nabla \boldsymbol{s}_u)^T)] \\
&\nabla \cdot \boldsymbol{s}_u = 0.
\end{aligned}$$

The key point here is that we adopt a *general* approach: we consider *any* design parameter a. Consequently, all the quantities involved (flow variables, material properties, coefficients, etc.) may simultaneously depend on a. All possible terms are actually included in the formulation. Hence, we have general and generic expressions for the sensitivity equations that account for all possible dependencies. The above equations are derived once and for all since the formulation is general. Specification of quantities such as ρ', μ' in the input file defines the parameter specific sensitivity equation. Note that some terms may vanish from the general equation. The user must provide the fluid properties ρ, μ, etc. for the flow along with their derivatives ρ', μ', etc. for the CSE. Note that these derivatives $(')$ must account for the total functional dependence. For example consider the eddy viscosity μ_t:

$$\mu_t = \rho C_\mu e^{2\mathcal{K}-\mathcal{E}}.$$

Its derivative is given by

$$\begin{aligned}\mu_t' &= (\rho' C_\mu + \rho C_\mu')e^{2\mathcal{K}-\mathcal{E}} + \rho C_\mu e^{2\mathcal{K}-\mathcal{E}}(2s_\mathcal{K} - s_\mathcal{E}) \\ &= \mu_t\left(\frac{\rho'}{\rho} + \frac{C_\mu'}{C_\mu} + 2s_\mathcal{K} - s_\mathcal{E}\right)\end{aligned}$$

where $s_\mathcal{K} = \frac{\partial \mathcal{K}}{\partial a}$ and $s_\mathcal{E} = \frac{\partial \mathcal{E}}{\partial a}$ are obtained from the solution of the transport equations given in the next subsection.

3.2 Turbulence sensitivity equations

Differentiation of the turbulence transport (3) and (4) with respect to design parameter a yields the continuous sensitivity equations for $s_\mathcal{K}$ and $s_\mathcal{E}$. Following the general approach, these generic equations take the form:

$$\begin{aligned}&\rho' \boldsymbol{u}\cdot\nabla\mathcal{K} + \rho \boldsymbol{s}_u\cdot\nabla\mathcal{K} + \rho\boldsymbol{u}\cdot\nabla s_\mathcal{K} \\ &\quad= \nabla\cdot\left[\left(\mu' + \frac{\mu_t'}{\sigma_k} - \frac{\mu_t\sigma_k'}{\sigma_k^2}\right)\nabla\mathcal{K} + \left(\mu + \frac{\mu_t}{\sigma_k}\right)\nabla s_\mathcal{K}\right] \\ &\qquad+ \left(\mu' + \frac{\mu_t'}{\sigma_k} - \frac{\mu_t\sigma_k'}{\sigma_k^2}\right)\nabla\mathcal{K}\cdot\nabla\mathcal{K} + 2\left(\mu + \frac{\mu_t}{\sigma_k}\right)\nabla\mathcal{K}\cdot\nabla s_\mathcal{K} \\ &\qquad+ e^{-\mathcal{K}}(\mu_t' P + \mu_t P' - \mu_t P s_\mathcal{K}) \\ &\qquad- \rho e^{\mathcal{E}-\mathcal{K}}\left(2\frac{\rho'}{\rho} + \frac{C_\mu'}{C_\mu} + s_\mathcal{K} - \frac{\mu_t'}{\mu_t}\right) + q_\mathcal{K}'\end{aligned}$$

and

$$\begin{aligned}&\rho' \boldsymbol{u}\cdot\nabla\mathcal{E} + \rho \boldsymbol{s}_u\cdot\nabla\mathcal{E} + \rho\boldsymbol{u}\cdot\nabla s_\mathcal{E} \\ &\quad= \nabla\cdot\left[\left(\mu' + \frac{\mu_t'}{\sigma_\epsilon} - \frac{\mu_t\sigma_\epsilon'}{\sigma_\epsilon^2}\right)\nabla\mathcal{E} + \left(\mu + \frac{\mu_t}{\sigma_\epsilon}\right)\nabla s_\mathcal{E}\right] \\ &\qquad+ \left(\mu' + \frac{\mu_t'}{\sigma_\epsilon} - \frac{\mu_t\sigma_\epsilon'}{\sigma_\epsilon^2}\right)\nabla\mathcal{E}\cdot\nabla\mathcal{E} + 2\left(\mu + \frac{\mu_t}{\sigma_\epsilon}\right)\nabla\mathcal{E}\cdot\nabla s_\mathcal{E} \\ &\qquad+ \rho C_1 C_\mu e^{\mathcal{K}-\mathcal{E}} P\left(\frac{\rho'}{\rho} + \frac{C_1'}{C_1} + \frac{C_\mu'}{C_\mu} + s_\mathcal{K} - s_\mathcal{E} + \frac{P'}{P}\right) \\ &\qquad- C_2\rho e^{\mathcal{E}-\mathcal{K}}\left(\frac{C_2'}{C_2} + \frac{\rho'}{\rho} + s_\mathcal{E} - s_\mathcal{K}\right) + q_\mathcal{E}'\end{aligned}$$

where the sensitivity of the production term is

$$P' = 2\nabla \boldsymbol{s}_u : (\nabla\boldsymbol{u} + (\nabla\boldsymbol{u})^T).$$

The sensitivities of the turbulence logarithmic variables are used for numerical computations. However, if the analysis requires the sensitivities of k and ϵ (i.e. s_k

and s_ϵ), the following transformation may be used:

$$s_k = k s_{\mathcal{K}},$$
$$s_\epsilon = \epsilon s_{\mathcal{E}}.$$

Once again we stress that the above equations are developed and implemented once and for all. It is the specification by the user of the derivatives of the physical properties and other coefficients (ρ', μ', C'_μ, C'_1, C'_2, σ'_k, σ'_ϵ, etc.) that defines the parameter specific sensitivity equations.

3.3 Sensitivity boundary conditions

The sensitivity boundary conditions are also derived by implicit differentiation of the flow boundary conditions (5–9). In this development, we assume that the boundary is parameter independent. The more general case of shape parameters is treated by Turgeon et al. (2000a) where a unified approach for shape and value parameters was developed for laminar flows. However, the computation of sensitivities for wall functions applied to a parameter dependent boundary (shape sensitivity) requires the evaluation of the second derivatives of the flow along the boundary of the computational domain. Obtaining accurate second derivatives is still an unresolved issue and a difficult problem. Therefore, we focus our attention on value parameters.

For a value parameter (fixed boundary), the Dirichlet boundary condition for the sensitivities corresponding to (5) is thus

$$\boldsymbol{s}_u = \boldsymbol{u}'_{bc} \quad \text{on } \Gamma_d.$$

For the outflow conditions (6), we get

$$-s_p + \hat{\boldsymbol{n}} \cdot \boldsymbol{\tau}'(\boldsymbol{u}) \cdot \hat{\boldsymbol{n}} = 0 \quad \text{and} \quad \boldsymbol{s}_u \cdot \hat{\boldsymbol{t}} = 0 \quad \text{on } \Gamma_n.$$

Similar manipulations are performed for the remaining boundary conditions.

For all parameters, the CSE have the same structure and the same type of boundary conditions as the flow equations. That is the CSE have Dirichlet (Neumann) conditions where the flow equations have Dirichlet (Neumann) conditions. This is important, since it results in the same structure for the variational form of both systems. This also implies that the CSE solver has the same code organization as the flow solver.

3.4 Sensitivity of wall boundary conditions

Wall functions provide boundary conditions for the flow. Again, the corresponding boundary conditions for the sensitivity equations are obtained by implicit differentiation of the wall functions. Differentiation of the no-penetration condition (16) leads to

$$\boldsymbol{s}_u \cdot \hat{\boldsymbol{n}} = 0$$

whereas the sensitivity of the shear stress is given by

$$\tau'_w = \rho' u_k u_{**} + \rho u'_k u_{**} + \rho u_k u'_{**}.$$

The sensitivities u'_{**} and u'_k appearing in this expression are obtained by differentiation of (12) and (13):

$$u'_{**} = \frac{u'_t}{u^+} - \frac{u_t u^{+\prime}}{u^{+2}}$$

$$u'_k = u_k \left(\frac{1}{4} \frac{C'_\mu}{C_\mu} + \frac{1}{2} s_{\mathcal{K}} \right)$$

where, from (10),

$$u^{+\prime} = \begin{cases} y^{+\prime} & \text{for } y^+ < y_c^+, \\ \frac{1}{\kappa}(-u^+ \kappa' + \frac{E'}{E} + \frac{y^{+\prime}}{y^+}) & \text{for } y^+ \geq y_c^+ \end{cases}$$

and, from (11),

$$y^{+\prime} = y^+ \left(\frac{\rho'}{\rho} + \frac{d'}{d} + \frac{u'_k}{u_k} - \frac{\mu'}{\mu} \right). \tag{18}$$

Finally, for the tangential component of velocity

$$u_t = u t_x + v t_y$$

we get

$$u'_t = s_u t_x + s_v t_y.$$

Here we have assumed that $t'_x = t'_y = 0$ because we consider only value parameters (i.e. parameter independent wall geometries). Note that even if the computational boundary is fixed, the distance to the wall d may vary. Thus, d is simply considered as a value parameter in the wall functions.

From (14) we deduce the following boundary condition for $s_{\mathcal{K}}$

$$\frac{\partial s_{\mathcal{K}}}{\partial n} = 0$$

which can be written in a form more suitable for the natural boundary conditions of the finite element formulation:

$$\left[\left(\mu' + \frac{\mu'_t}{\sigma_k} - \frac{\mu_t \sigma'_k}{\sigma_k^2} \right) \nabla \mathcal{K} + \left(\mu + \frac{\mu_t}{\sigma_k} \right) \nabla s_{\mathcal{K}} \right] \cdot \hat{\boldsymbol{n}} = 0.$$

Finally, the boundary condition for $s_{\mathcal{E}}$ is

$$s_{\mathcal{E}} = 3 \frac{u'_k}{u_k} - \frac{\kappa'}{\kappa} - \frac{d'}{d}.$$

Here again, the above equations for the sensitivity boundary conditions are derived once and for all. The specification of sensitivities of the coefficients appearing in the boundary conditions (ρ', μ', d', κ', and e') define the appropriate parameter specific boundary conditions for the sensitivity equations.

3.5 A sample sensitivity system: C_2 as a parameter

We now provide an example of the system of sensitivity equations for the case where the turbulence closure coefficient C_2 is the parameter of interest. The sensitivity equations for the continuity and momentum equations are

$$\begin{aligned}\nabla \cdot \boldsymbol{s}_u &= 0,\\ \rho \boldsymbol{s}_u \cdot \nabla \boldsymbol{u} + \rho \boldsymbol{u} \cdot \nabla \boldsymbol{s}_u &= -\nabla s_p + \nabla \cdot [\mu_t'(\nabla \boldsymbol{u} + (\nabla \boldsymbol{u})^T)\\ &\quad + (\mu + \mu_t)(\nabla \boldsymbol{s}_u + (\nabla \boldsymbol{s}_u)^T)]\end{aligned}$$

note that $\rho' = \mu' = C_\mu' = 0$ since ρ, μ and C_μ do not depend on C_2.

For the turbulence equations, we obtain the following sensitivity equations:

$$\begin{aligned}\rho \boldsymbol{s}_u \cdot \nabla \mathcal{K} + \rho \boldsymbol{u} \cdot \nabla s_{\mathcal{K}} &= \nabla \cdot \left[\frac{\mu_t'}{\sigma_k}\nabla \mathcal{K} + \left(\mu + \frac{\mu_t}{\sigma_k}\right)\nabla s_{\mathcal{K}}\right]\\ &\quad + \frac{\mu_t'}{\sigma_k}\nabla \mathcal{K} \cdot \nabla \mathcal{K} + 2\left(\mu + \frac{\mu_t}{\sigma_k}\right)\nabla \mathcal{K} \cdot \nabla s_{\mathcal{K}}\\ &\quad + e^{-\mathcal{K}}(\mu_t' P + \mu_t P' - \mu_t P s_{\mathcal{K}}) - \rho e^{\mathcal{E}-\mathcal{K}}\left(s_{\mathcal{K}} - \frac{\mu_t'}{\mu_t}\right)\end{aligned}$$

and

$$\begin{aligned}\rho \boldsymbol{s}_u \cdot \nabla \mathcal{E} + \rho \boldsymbol{u} \cdot \nabla s_{\mathcal{E}} &= \nabla \cdot \left[\frac{\mu_t'}{\sigma_\epsilon}\nabla \mathcal{E} + \left(\mu + \frac{\mu_t}{\sigma_\epsilon}\right)\nabla s_{\mathcal{E}}\right]\\ &\quad + \frac{\mu_t'}{\sigma_\epsilon}\nabla \mathcal{E} \cdot \nabla \mathcal{E} + 2\left(\mu + \frac{\mu_t}{\sigma_\epsilon}\right)\nabla \mathcal{E} \cdot \nabla s_{\mathcal{E}}\\ &\quad + \rho C_1 C_\mu e^{\mathcal{K}-\mathcal{E}} P\left(s_{\mathcal{K}} - s_{\mathcal{E}} + \frac{P'}{P}\right)\\ &\quad - C_2 \rho e^{\mathcal{E}-\mathcal{K}}\left(\frac{1}{C_2} + s_{\mathcal{E}} - s_{\mathcal{K}}\right)\end{aligned}$$

where the sensitivity of the production term is

$$P' = 2\nabla \boldsymbol{s}_u : (\nabla \boldsymbol{u} + (\nabla \boldsymbol{u})^T)$$

and the sensitivity of the eddy viscosity is

$$\mu_t' = \mu_t(2s_{\mathcal{K}} - s_{\mathcal{E}}),$$

where again simplifications occur because $\rho' = \mu' = C_\mu' = 0$. Furthermore, we also have $\sigma_k' = \sigma_\epsilon' = C_1' = 0$.

The above system is subject to the following boundary conditions. For the momentum equations, the sensitivity of the normal velocity is set to zero and the sensitivity of the shear stress is given by

$$\tau_w' = \rho u_k' u_{**} + \rho u_k u_{**}',$$

where

$$u'_k = \frac{1}{2} u_k s_{\mathcal{K}},$$

$$u'_{**} = \frac{u'_t}{u^+} - \frac{u_t u^{+\prime}}{u^{+2}}$$

and

$$u^{+\prime} = \begin{cases} y^{+\prime} & \text{for } y^+ < y_c^+, \\ \frac{1}{\kappa} \frac{y^{+\prime}}{y^+} & \text{for } y^+ \geq y_c^+, \end{cases}$$

$$y^{+\prime} = y^+ \frac{u'_k}{u_k}.$$

For the tangential velocity ($u_t = u t_x + v t_y$), we get

$$u'_t = s_u t_x + s_v t_y.$$

Finally, the boundary conditions for $s_{\mathcal{K}}$ and $s_{\mathcal{E}}$ are:

$$\frac{\partial s_{\mathcal{K}}}{\partial n} = 0,$$

$$s_{\mathcal{E}} = 3 \frac{u'_k}{u_k}.$$

4 Boundary conditions for shape parameters

The previous development of boundary conditions is valid for value parameters only, that is for parameters whose variations do not affect the geometry of the computational domain. This section highlights some of the difficulties encountered with the SEM when dealing with shape parameters. We begin our discussion with Dirichlet conditions and then proceed to Neumann or flux conditions.

For shape parameters the shape of the boundary and the applied Dirichlet condition may both depend on the parameter. The shape of the boundary can be described by the following parametrisation

$$\Gamma_{d_i} = \{(x_i(t; a), y_i(t; a)) \mid t \in [0, 1],\ a \in D \subseteq \mathbb{R}^n\}, \quad i = 1, \ldots, m,$$

while Dirichlet boundary conditions on Γ_{d_i} can be written for the components (u, v) of $\mathbf{u}$ as

$$u(x_i(t; a), y_i(t; a); a) = u_{\text{bc}}(x_i(t; a), y_i(t; a); a) \tag{19}$$

$t \in [0, 1]$, and similarly for v. Differentiating (19) with respect to a and suppressing the arguments yields the formula

$$\frac{\partial u}{\partial x}\frac{\partial x_i}{\partial a} + \frac{\partial u}{\partial y}\frac{\partial y_i}{\partial a} + \frac{\partial u}{\partial a} = \frac{D u_{\text{bc}}}{D a}.$$

This can be solved for the sensitivity variable $s_u = \frac{\partial u}{\partial a}$ to determine the CSE boundary condition corresponding to the flow boundary condition in (19):

$$s_u = -\nabla u \cdot \Pi_a + \frac{Du_{\text{bc}}}{Da}, \tag{20}$$

where $\Pi_a \equiv (\frac{\partial x_i}{\partial a}, \frac{\partial y_i}{\partial a})$ is known (by assumption) along Γ_{d_i}. Note that when $\Pi_a \neq \mathbf{0}$, $\nabla \mathbf{u}$ must be evaluated at the boundary to compute the Dirichlet condition for the sensitivity. It is a well known fact that the finite element flow derivatives are less accurate at the boundary than in the core of the flow. Hence, Dirichlet boundary conditions for shape sensitivities are at best as accurate as the flow derivatives. This loss of accuracy can be partly compensated by smoothing of the flow derivatives and by mesh adaptation. The extraction of high order derivatives at the boundary remains an open and unsolved issue.

This issue becomes compounded if we look at Neumann conditions on parameter dependent boundaries. In this case second derivatives of the flow variables are required to find the flux boundary condition for the sensitivities and are more problematic to compute than first derivatives. Consider for example the zero normal derivative condition for $\mathcal{K}$, which we write in the following fashion

$$\nabla \mathcal{K} \cdot \hat{\mathbf{n}} = 0$$

The implicit differentiation on the above expression yields the required Neumann boundary condition for the sensitivity. However, one must account for the fact that both $\mathcal{K}$ and $\hat{\mathbf{n}}$ depend on a. This operation yields

$$\frac{D}{Da}(\nabla \mathcal{K}) \cdot \hat{\mathbf{n}} + \nabla \mathcal{K} \cdot \frac{D\hat{\mathbf{n}}}{Da} = 0$$

or

$$(\nabla \mathcal{K} + \nabla s_{\mathcal{K}}) \cdot \hat{\mathbf{n}} = -\kappa \nabla \mathcal{K} \cdot \frac{\mathbf{D}\hat{\mathbf{n}}}{\mathbf{Da}} - \left[\frac{\partial}{\partial \mathbf{x}}(\nabla \mathcal{K}) \frac{\partial \mathbf{x_b}}{\partial \mathbf{a}} + \frac{\partial}{\partial \mathbf{y}}(\nabla \mathcal{K}) \frac{\partial \mathbf{y_b}}{\partial \mathbf{a}} \right] \cdot \hat{\mathbf{n}}.$$

The need to evaluate first and second derivatives of $\mathcal{K}$ at the boundary is an outstanding issue and constitutes a major challenge for the CSE approach.

4.1 Scaled sensitivities

One use of sensitivities is the determination of the influence of parameter changes on the flow. It is difficult to determine this dependence from the raw information such as $\boldsymbol{s}_u$, s_p and $s_{\mathcal{K}}$ since parameter often have different units. Thus, for design parameters a and b, comparing $\frac{\partial u}{\partial a}$ and $\frac{\partial u}{\partial b}$ can be misleading. A solution to this problem is to scale the sensitivity values by the nominal (reference) values of the parameter (Blackwell et al. 1998). The resulting *scaled sensitivities* have the form

$$\frac{\partial \boldsymbol{u}}{\partial a} a_0, \qquad \frac{\partial p}{\partial a} a_0, \qquad \text{etc.},$$

where a_0 is the nominal value of the design parameter a. In this way, comparing $\frac{\partial u}{\partial a} a_0$ with $\frac{\partial u}{\partial b} b_0$ is more meaningful.

5 Implementation

The flow equations and the CSE are solved in the same software using an adaptive finite element method. The solver is partly segregated. The steady-state momentum and continuity equations are solved in a coupled manner by Newton iteration with a frozen eddy viscosity field. The turbulence kinetic energy equation is then solved by Newton's method using the most recent velocity field. Finally, the dissipation rate equation is solved by Newton's method using the most recent estimates of the velocity and TKE. Two to three Sub-iterations between the turbulence equations speed up the overall fixed point algorithm. Element matrices are constructed using a numerical Jacobian technique. When needed, stabilization terms are added to the standard Galerkin formulation. The system matrices are stored in a compacted skyline format and solved by Gaussian elimination. This is a very effective strategy. However, it a memory greedy approach.

The equations are discretized with the 7-node Crouzeix–Raviart element which uses enriched quadratic basis function for velocity and a linear discontinuous pressure approximation. The continuity equation is handled via an augmented Lagrangian formulation. Turbulence variables are discretized with quadratic polynomials.

Wall function boundary conditions are fully coupled to the momentum and continuity equation. Their contributions are linearized by Newton's method as follows. The universal velocity profile is

$$u^+ = \frac{1}{\kappa}\ln(Ey^+)$$

while the TKE velocity scale is

$$u_k = C_\mu^{\frac{1}{4}} k^{\frac{1}{2}}$$

which yields

$$\begin{aligned} u^+ &= u/u_{**} \quad \text{and} \quad y^+ = d\rho u_k/\mu \neq f(u), \\ \frac{u}{u_{**}} &= \frac{1}{\kappa}\ln(Ey^+), \\ u_{**} &= u\left[\frac{\kappa}{\ln(Ey^+)}\right]. \end{aligned}$$

This last expression is an explicit relation between k and u_{**}.

The boundary condition for the mean velocity are

$$\begin{aligned} \tau_w &= \rho u_k u_{**}(u), \\ \boldsymbol{u}\cdot\hat{\boldsymbol{n}} &= 0 \end{aligned}$$

which can be re-written as

$$\tau_w = \left[\frac{\rho u_k \kappa}{\ln(Ey^+)}\right] u \quad \text{linear in } u.$$

The wall function elemental matrix system is obtained by a finite difference evaluation of the Jacobian

$$\frac{\partial \tau}{\partial u} = \frac{\tau(u_0 + \delta) - \tau(u_0 - \delta)}{2\delta}.$$

Note that the sensitivity system is linear, yet it is solved by block Gauss–Seidel. This is not the most efficient approach, however it is compatible with that of our research flow code. Typically, the solution of the system of equation for one sensitivity parameter takes 15% of the CPU time for evaluating the flow. Much more efficient commercial algorithms exist which reduce this cost to a few percent of a flow solve (1 to 5%) (Godfrey and Cliff 2001). However, the formulation of Godfrey and Cliff (2001) is not as general as the one presented here.

The adaptive remeshing procedure used here is modeled after that proposed by Peraire et al. (1987) and is described in more details by Ilinca et al. (1996, 1997a). The procedure clusters grid points in regions of rapid variations of all dependent variables: velocity, pressure, logarithmic turbulence variables, and the eddy viscosity. Error estimates are obtained by a local least squares reconstruction of the solution derivatives (Zienkiewicz and Zhu 1992a, 1992b). For the velocity field, the strain rate tensor is used for error estimation. An error estimate of the pressure solution is obtained by a local projection of the pressure field itself. Error estimates are obtained for the turbulence variables by projecting the finite element derivatives of $\mathcal{K}$ and $\mathcal{E}$ into a continuous field. Finally, an error estimate for the eddy viscosity is also constructed since slowly varying fields of $\mathcal{K}$ and $\mathcal{E}$ can result in rapid variation of the eddy viscosity. This is very important to the success of adaptation in turbulent flows since the eddy viscosity is the sole mechanism for diffusion of momentum and turbulence kinetic energy by turbulent fluctuations. See Ilinca et al. (1997a, 1997b); Pelletier and Ilinca (1997) for examples and some discussions of these issues.

Once the error estimates are obtained for all variables, a better mesh must be designed. In our approach, all variables are analyzed and contribute to the mesh adaptation process. For this, an error estimate is obtained separately for each dependent variable. The mesh characteristics (element size) are derived for each variable on a given element. The mesh is designed so as to result in a reduction of the error by a user-specified factor. The minimum element size predicted by each of the dependent variable is selected on each element. The process of solution, error estimation, and remeshing is repeated until satisfactory accuracy is achieved. Details of this algorithm have been presented previously in (Ilinca 1996; Turgeon 1997; Ilinca and Pelletier 1997).

If an adaptive mesh generation routine is used for the flow, then the CSEs only need to be computed on the finest mesh. However, we choose to solve the CSEs at each cycle of mesh adaptation and use error estimates of all the sensitivity variables in the mesh refinement scheme (Borggaard and Pelletier 1998; Pelletier et al. 2002). This allows a better control of the sensitivity solution accuracy because a good adaptive mesh for the flow solution may not necessarily be well adapted for the sensitivity solution (Borggaard and Pelletier 1998; Pelletier et al. 2002).

6 Numerical results

In this section, numerical results are presented for three applications: decay of grid turbulence, flow over a backward facing step, and flow over a flat plate. The first example verifies the formulation and implementation, whereas the remaining problems illustrate the flexibility of the proposed methodology and demonstrate a variety of different applications of sensitivities. The sensitivity parameters considered are the closure coefficients of the k–ϵ model of turbulence and the coefficients appearing in the wall functions.

6.1 Verification: grid turbulence

In CFD or any other field based on numerical methods, *verification* should precede applications (Roache 1998). Verification is performed on problems possessing a closed form solution. Two verifications of our code were reported in Turgeon et al. (2001a) for sensitivity analysis of turbulent flows. However, for completeness, another verification example is included here. The problem considered is the decay of grid turbulence in a uniform flow, as presented by Ilinca et al. (1998), which has an analytical solution. We set μ and C_μ to extremely low values so that diffusion terms become negligible. The exact solution is given by:

$$
\begin{aligned}
u &= 1, \\
v &= 0, \\
p &= 0, \\
k &= \epsilon_0 \left(\frac{\epsilon_0}{k_0} \right)^{-\frac{C_2}{C_2 - 1}} \left[(C_2 - 1)x + \frac{k_0}{\epsilon_0} \right]^{-\frac{1}{C_2 - 1}}, \\
\epsilon &= \epsilon_0 \left(\frac{\epsilon_0}{k_0} \right)^{-\frac{C_2}{C_2 - 1}} \left[(C_2 - 1)x + \frac{k_0}{\epsilon_0} \right]^{-\frac{C_2}{C_2 - 1}}
\end{aligned}
$$

where k_0 and ϵ_0 are the turbulence kinetic energy and the turbulence dissipation at the inlet ($x = 0$). The computational domain extends from $(0, 0)$ to $(1, 0.2)$. Dirichlet boundary conditions are applied at the inlet, while zero Neumann conditions are applied everywhere else. For the sensitivity computations, C_2 is the parameter and the exact sensitivities are obtained by differentiation of the exact flow solution.

Figure 2 shows the distributions of $\mathcal{K}$, $\mathcal{E}$, $s_\mathcal{K}$, and $s_\mathcal{E}$ along the line $y = 0.1$ (bisecting the domain). These results were obtained after five cycles of adaptation on a mesh containing 1299 nodes. As can be seen, the overlap is so nearly perfect that the numerical predictions are indistinguishable from the exact solutions. This confirms the accuracy of predictions and ability of the code to deliver the right solution to the equations for both the flow and its sensitivities.

6.2 Application: backward facing step

The first application is the flow over a backward facing step, studied experimentally by Kim (1978). The domain is presented in Figure 3(a). For this dimensionless simulation, the Reynolds number is $\mathrm{Re} = 47\,625$ based on the step height L.

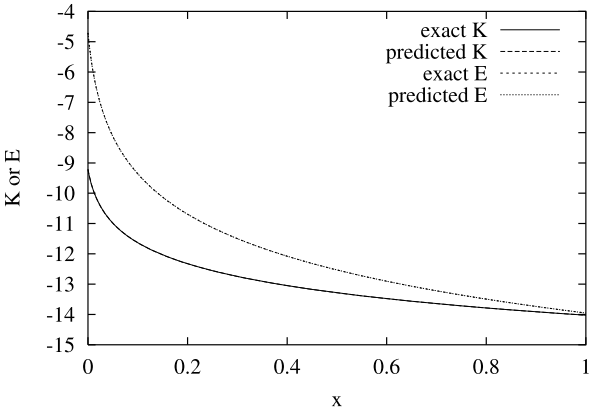

a) flow ($\mathcal{K}$ and $\mathcal{E}$)

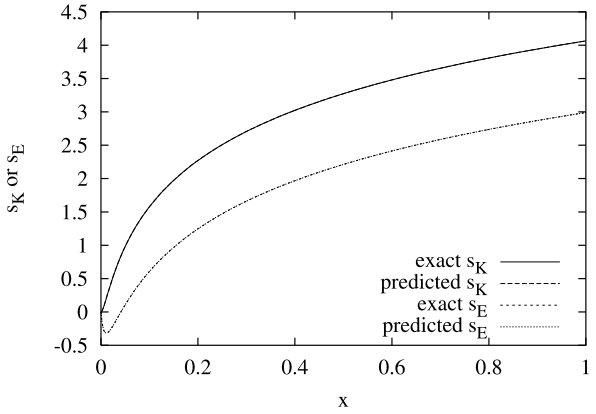

b) sensitivities ($s_{\mathcal{K}}$ and $s_{\mathcal{E}}$)

Fig. 2 Grid turbulence: solution at $y = 0.1$

Because little or no experimental information is available to set the boundary conditions, we assume a uniform flow at the inlet. For lack of details on the experiment at the inflow, constant Dirichlet boundary conditions are applied at the inlet: $u = 1$, $v = 0$, $k = 0.005$, and $\epsilon = 0.01$. At the outlet, $v = 0$, the normal stress is set to zero, and the normal derivatives of k and ϵ are also set to zero. The other boundaries use wall functions, with distances d to the wall given in Table 2. These values were selected to ensure that d^+ lies in its interval of validity ($30 < d^+ < 300$). For the sensitivity computations, five parameters are considered: the closure coefficients of the k–ϵ model of turbulence, that is, C_μ, C_1, C_2, σ_k, and σ_ϵ.

Figure 3 shows the final adapted mesh and some solution contours. This mesh is obtained after 4 cycles of adaptation and contains 60 027 nodes. A high level of refinement exists near the corner of the expansion, in the shear layer and near the bottom wall. Such levels of refinement are in agreement with sharp solution gradients (clustered solution contour lines). Note that the sensitivity $s_{\mathcal{K}}$ exhibits a very sharp front. However, we can see that the mesh upstream of the expansion and along the

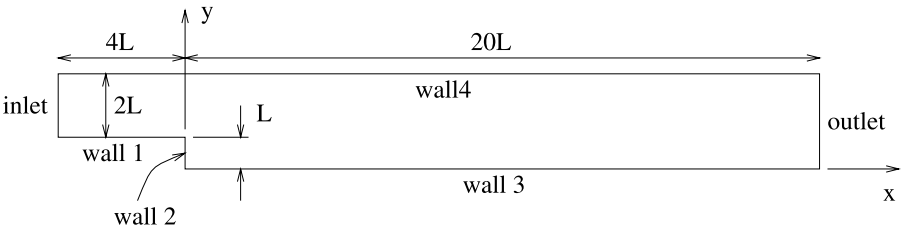

a) Domain definition

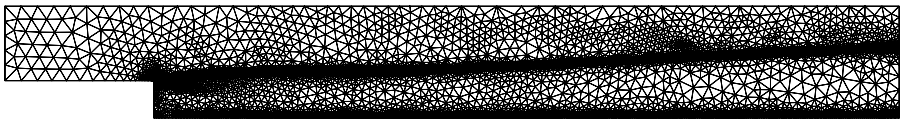

b) final mesh

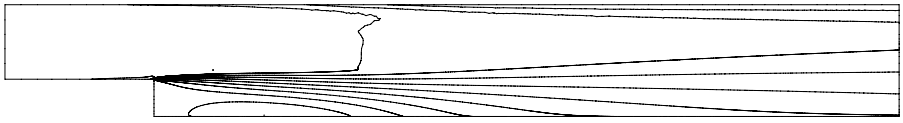

c) u

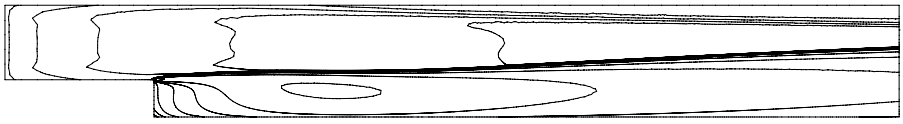

d) $\mathcal{K}$

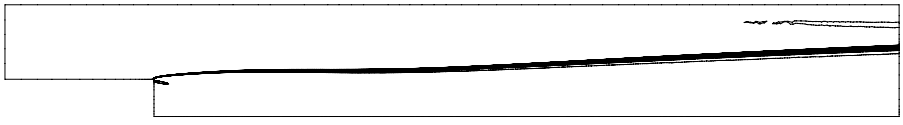

e) $\frac{\partial \mathcal{K}}{\partial C_1}$

Fig. 3 Backward facing step: solution on final mesh

upper wall is not as refined. With a 2-velocity scales wall functions, the Reynolds stresses depend on the turbulence kinetic energy k whose value will increase if the production term $P(\boldsymbol{u})$ increases. This will only occur if the velocity gradients become large. As can be seen from 3(c) the velocity gradients are not very large on the top wall. The same is true of the face of the step. The stagnation point of recirculation zone induces large velocity gradients and more production of k. Additional adaptive cycles would likely lead to grid refinement along walls 1 and 4. See Lacasse et al. (2001) for a detailed analysis of these effects and observations in the case of the turbulent flow over a flat plate.

Note also that the mesh is not refined along the streamline separating the recirculation zone from the core flow. This is due to the fact that the error estimator tags

Table 2 Distances to the wall for the backward facing step.

Wall	Distance d
1	0.04
2	0.05
3	0.025
4	0.05

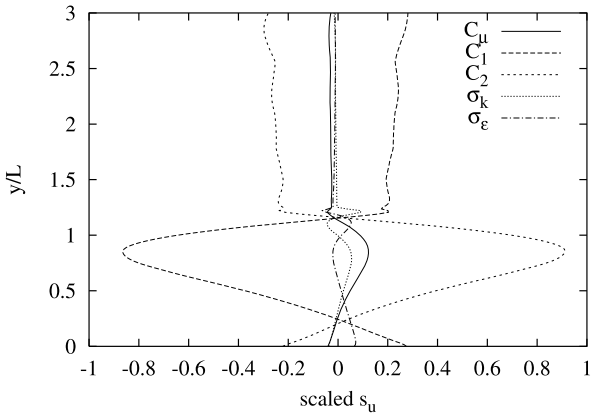

Fig. 4 Backward facing step: profiles of scaled sensitivities of u with respect to closure coefficients at $x/L = 8/3$

for refinement regions where the solution fields exhibit the highest curvature. The flow in the vicinity of the separation streamline is too smooth to trigger mesh refinement at this level of resolution. If more cycles of grid adaption were performed, the global errors would be reduced sufficiently that local errors near the recirculation edge would trigger refinement. However the flow features in this region are so weak that this would only occur on much finer grids.

Scaled sensitivities of u at $x/L = 8/3$ are plotted in Fig. 4. Note that this line intersects the recirculation zone (which ends at $x/L \sim 6.4$). It is clear from this figure that C_1 and C_2 have the most significant influence on the velocity u. Moreover, they seem to have a very similar effect, but with opposite signs. On the other hand, the coefficients σ_k and σ_ϵ have the smallest effects. Scaled sensitivities are thus useful for identifying dominant parameters.

We now use sensitivity information to perform an uncertainty analysis. There are many sources of uncertainty for the case at hand:

- model uncertainty,
- the use of a linear eddy viscosity model,
- inflow boundary conditions,
- closure coefficients,
- wall function parameters.

Model uncertainty is linked to the choice of turbulence model used for simulation. The use of a linear eddy viscosity model falls in the category of model uncertainty. Clearly, this is beyond the scope of sensitivity analysis. Model uncertainty is bet addressed through *validation*, as described by Roache (1998). Validation involves com-

parison with experimental data to determine whether the mathematical PDE model of the flow is a good representation of the physics at hand.

Our applications focuses on the closure coefficients and the parameters appearing in wall functions. We have selected these for two reasons. First, they constitute a good example of how sensitivity analysis can be used in the context of turbulence modeling. Indeed, sensitivities provide a richer base of information on which a modeler can rely for interpreting his simulation data. Secondly, these parameters fall in the category of value parameters which do not affect the geometry of the computational domain. Shape parameters are beyond the scope of this paper due to the special challenges for computational the present. These difficulties were briefly discussed earlier in the paper. Finally, inflow boundary conditions were not the subject of sensitivity analysis for brevity's sake.

A Taylor series expansion is used to cascade the uncertainties in the input parameters C_μ, C_1, C_2, σ_k, and σ_ϵ into the CFD solution. The net result is an uncertainty estimate on the flow solution itself. Thus we have:

$$\Delta u \leq \left|\frac{\partial u}{\partial C_\mu}\right|\Delta C_\mu + \left|\frac{\partial u}{\partial C_1}\right|\Delta C_1 + \left|\frac{\partial u}{\partial C_2}\right|\Delta C_2 + \left|\frac{\partial u}{\partial \sigma_k}\right|\Delta \sigma_k + \left|\frac{\partial u}{\partial \sigma_\epsilon}\right|\Delta \sigma_\epsilon \qquad (21)$$

where ΔC_μ is the uncertainty on C_μ, and so on. We know that the values of the closure coefficients are not *exact* or *perfect*. However, it is not an easy task to quantify their true uncertainty. No information is available concerning the uncertainty of the coefficients listed in Table 1. If one assumes that all digits given in Table 1 are numerically significant, then one can infer, as a first approximation, that these coefficients are accurate to within one half unit of the rightmost digit (Gerald and Wheatley 1998; Burden et al. 1981; Ralston and Abramowitz 1981). Table 3 summarizes the uncertainties in the coefficients used in the present study. Note that the "accuracy" of the coefficients is probably lower than that.

A note of caution is in order, closure coefficients are not a set of independent parameters. Hence, one should be careful in interpreting the results of the uncertainty cascade through the CFD if all parameters are incorporated in (21). Furthermore, the uncertainty cascade relies on a linear Taylor series, hence each parameter uncertainty should be small with respect to the mean value of its design parameter.

Figure 5 presents the prediction of the horizontal component of velocity at two different locations: $x/L = 8/3$ and $x/L = 8$. These plots include the uncertainty bands and the experimental measurements. First of all, we see that the predictions are in good agreement with the experiments. Furthermore, the uncertainty bands do not overlap with the experimental points (which contain uncertainties as well). Thus, the assumed uncertainties in the coefficient values do not explain the differences observed between numerical results and experimental measurements. In fact, the uncertainties on u are small. This is expected since the uncertainties on the coefficients are relatively small. Because (21), used to cascade parameter uncertainties through

Table 3 Assumed uncertainties of the closure coefficients

	ΔC_μ	ΔC_1	ΔC_2	$\Delta \sigma_k$	$\Delta \sigma_\epsilon$
Absolute uncertainty	0.005	0.005	0.005	0.05	0.05
Relative uncertainty	5.5%	0.35%	0.26%	1%	3.8%

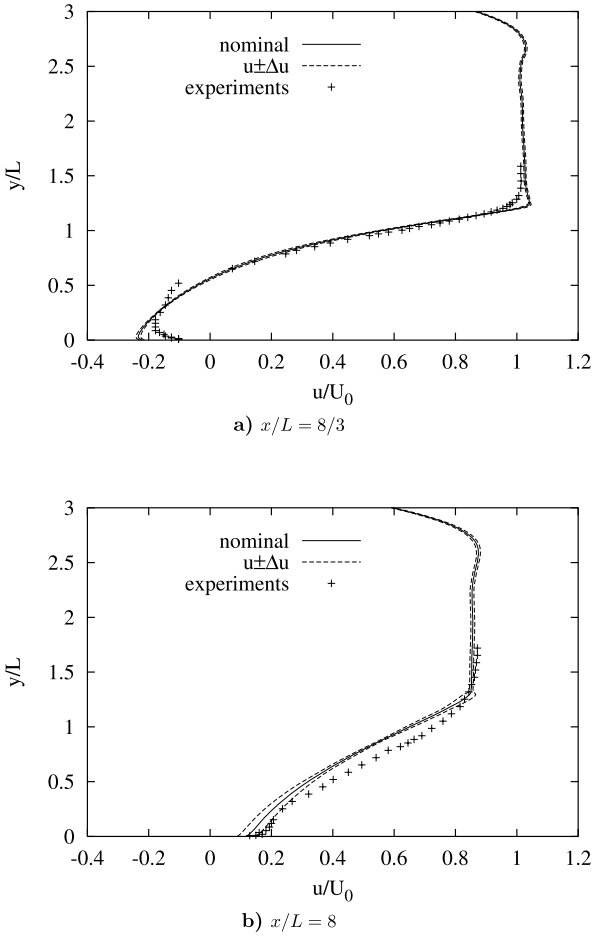

Fig. 5 Backward facing step: profiles of u and its predicted uncertainty intervals

the CFD, is linear increasing the input uncertainties by a factor of 10 would result in uncertainty bands 10 times large than those plotted on Fig. 5. However, this would make the uncertainty on C_μ equal to 55% which is beyond the domain of validity of (21); that is the uncertainty must be small with respect to the mean value of the parameter of interest.

Similar comparisons were performed for the turbulence kinetic energy. Figure 6 presents the scaled sensitivities of k at $x/L = 2.3$ and 5.8. Note that the distribution of k above the shear layer (i.e. in the core of the flow) is insensitive to the closure coefficients. Here, C_1 and C_2 are the dominant (turbulence) parameters. This is especially true in the recirculation zone ($x/L = 2.3$) and is less pronounced farther downstream. At $x/L = 2.3$, the peak of $C_1 \frac{\partial k}{\partial C_1}$ is approximately 7 times larger than k, indicating a large sensitivity. Craig and Venter (1999) reported similar observation about the effects of C_1 and C_2 on the location of the separation point on an airfoil.

Figures 7(a) and 7(b) compare the numerical predictions of k (together with uncertainty bands) to the experimental measurements of Kim (1978), who provides $\overline{u'^2}$

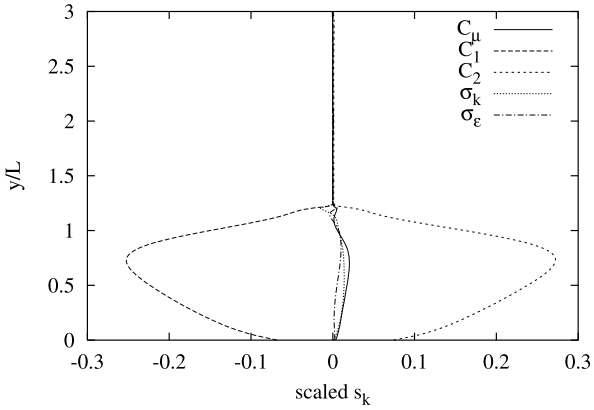

Fig. 6 Backward facing step: profiles of scaled sensitivities of k with respect to closure coefficients

and $\overline{v'^2}$, but not k. For the purpose of comparison, we approximate the experimental value of k as

$$k = \frac{1}{2}(\overline{u'^2} + \overline{v'^2}), \tag{22}$$

which is an underestimation (we neglect $\overline{w'^2}$). Clearly, the predictions are poor, even if we consider the uncertainties. There is an over-production of turbulence downstream of the expansion. Additionally, diffusion effects have not propagated k far enough into the main flow (above $y/L = 1.5$) when comparing to the experiments.

Another interesting distribution to observe is the skin friction coefficient C_f. The scaled sensitivities of C_f , with respect to the closure coefficients, along the bottom wall are plotted in Fig. 8. This provides information on the relative importance of the closure coefficients throughout the domain. The y-axis is labeled in a generic fashion because there is one curve for each of the closure coefficients studied here. Not surprisingly, C_f is most sensitive to C_1 and C_2. The sensitivities are maximum

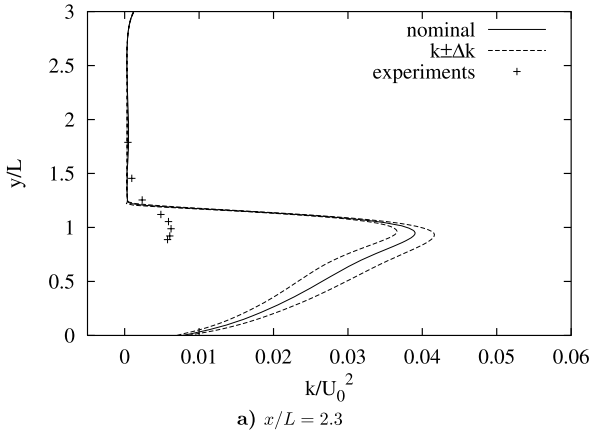

Fig. 7 Backward facing step: profiles of k and its predicted uncertainty intervals

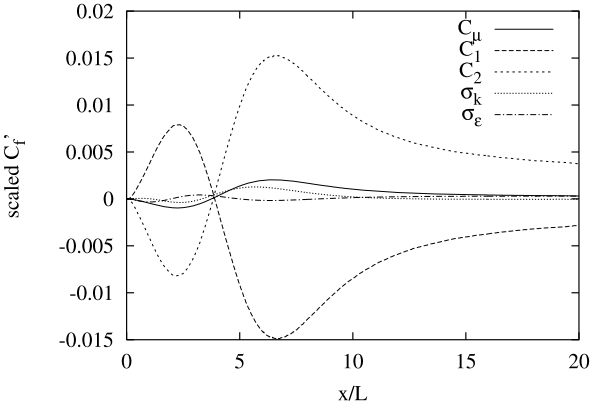

Fig. 8 Backward facing step: scaled sensitivities of C_f with respect to closure coefficients

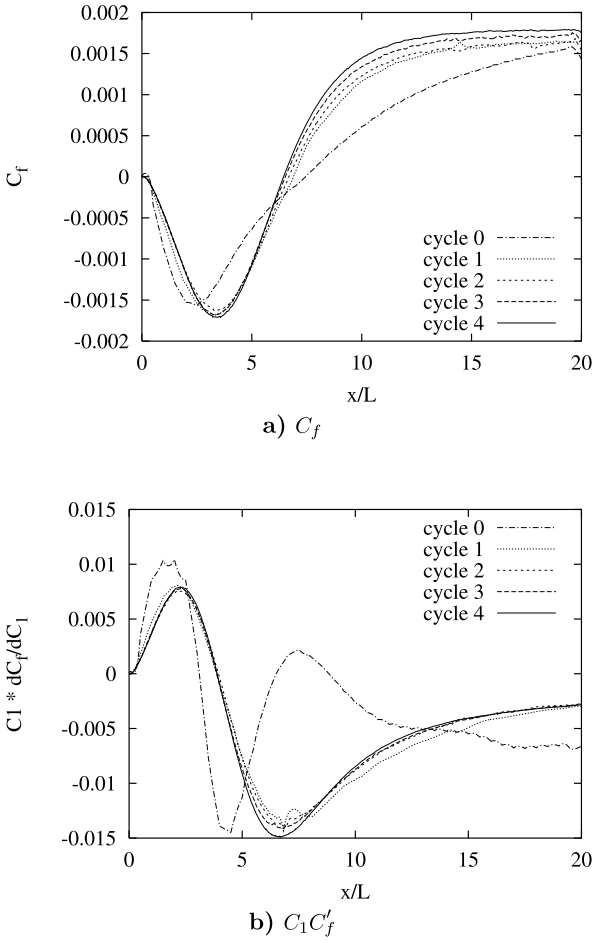

Fig. 9 Backward facing step: grid convergence of C_f and $C_1 \frac{\partial C_f}{\partial C_1}$

for x/L around 6 or 7, which corresponds to the reattachment point. On the other hand, sensitivities are very small around $x/L = 4$ where C_f exhibits a minimum (see Fig. 9).

The discussion would not be complete without a grid convergence study. Figure 9 provides the convergence history of C_f and a typical scaled sensitivity, $C_1 \frac{\partial C_f}{\partial C_1}$, with mesh adaptation. Both quantities are almost grid converged, with only small variations on the final meshes. More refinement would be desirable but was impossible due to computer memory limitations (the system matrices are stored in a compacted skyline format and the linear systems solved by Gaussian elimination; a memory greedy approach). In the context of uncertainty analysis with very small data uncertainties, it is preferable to reduce these numerical errors to negligible levels to ensure a rigorous uncertainty assessment. This is not perfectly achieved here even with our mesh adaptation strategy. Note also that mesh convergence is achieved on coarser meshes for some variables, while finer meshes may be required for other sensitivity parameters. Thus results must be interpreted with some care. However, the numerical errors are smaller than the uncertainties so that the present predictions are fairly reliable.

A single computation on a single non-adapted mesh would most likely lead to worse results unless the mesh were very fine, in which case the CPU cost would likely be prohibitively large compared to that of an adaptive computation.

6.3 Application: flat plate

The second application we investigate is the development of a turbulent boundary layer over a flat plate at $\mathrm{Re} = 2 \times 10^6$. This flow was studied by Lacasse et al. (2001) and sensitivities with respect to free-stream velocity were computed by Turgeon et al. (2004). Here we use the same configuration and boundary conditions, but use other design parameters for sensitivity analysis.

The first series of computations considers the closure coefficients C_μ, C_1, C_2, σ_k, and σ_ϵ as design parameters. Figure 10 compares the prediction of the skin friction coefficient along the plate to three correlations (Schlichting 1979; White 1974; Schultz-Grunow 1941). An uncertainty band is added to the finite element prediction using the same approach and data uncertainty as for the backward facing step. Globally, the agreement between predictions and correlations is good. The general trend is a slight under-prediction of C_f except near the leading edge. The uncertainty band is too narrow to account for the observed discrepancy between prediction and correlation. Larger perturbations in the values of the closure coefficients would be needed to capture the experimental measurements. Table 4 lists the contributions of each parameter to the uncertainty in the skin friction ΔC_f at the station $x/L = 0.8$. At this location, the finite element prediction is $C_f = 3.11 \times 10^{-3}$ whereas Schultz-Grunow's correlation gives $C_f = 3.31 \times 10^{-3}$. Hence, the discrepancy is about 6%. Observe that the variables, σ_ϵ and C_μ contribute the bulk of the uncertainty, whereas σ_k has only a small influence on the uncertainty in C_f. The total uncertainty is 4.17×10^{-5}, one fifth of the discrepancy between the prediction and the Schultz-Grunow correlation. Matching the correlation by overlapping it with the uncertainty bands would require a five fold increase in the parameter uncertainty (2.5 units of the rightmost digit instead of the 0.5 units we assume). These increments should be considered as very high given the rather small discrepancy (6%) in C_f. Nominal increments in C_μ, σ_k, and σ_ϵ do not explain the discrepancy in our numerical simulation.

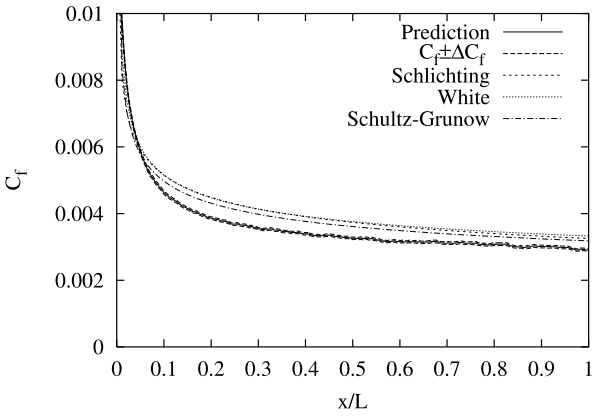

Fig. 10 Skin friction coefficient on a flat plate

Table 4 Contributions to uncertainties on C_f at $x/L = 0.8$

Parameter	$10^3 C'_f$	$10^5 \Delta C_f$ (uncertainty)
C_μ	2.58	1.29
C_1	−0.88	0.44
C_2	1.22	0.61
σ_k	0.04	0.19
σ_ϵ	0.33	1.64

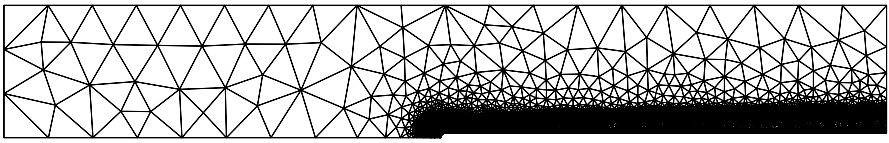

a) Final adapted mesh

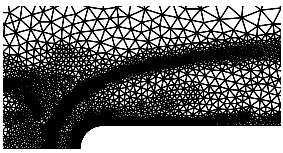

b) Zoom of the final mesh

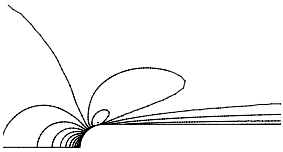

c) u

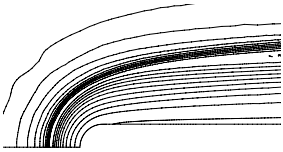

d) $\frac{\partial \mathcal{K}}{\partial C_1}$

Fig. 11 Flat plate: final mesh and solution

Figure 11 illustrates the final adapted mesh for this problem. Contours of the solution explain the grid point concentration. The velocity needs refinement near the leading edge and along the plate where the boundary layer develops. The outer band of refinement is dictated by turbulence variables, especially by $\frac{\partial \mathcal{K}}{\partial C_1}$.

The second sensitivity analysis for the flat plate problem focuses on the effect of the parameters κ, E, and d appearing in the wall function. Figure 12 plots the grid converged distribution of the scaled sensitivities of C_f. Of these parameters, the Kár-

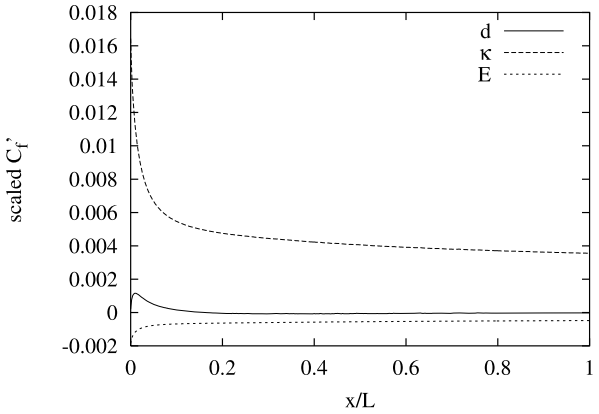

Fig. 12 Flat plate: scaled sensitivities C_f with respect to wall function parameters

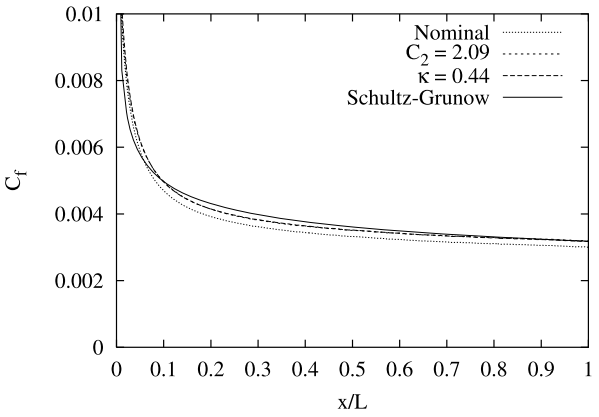

Fig. 13 Flat plate: C_f for perturbed values of parameters

mán constant κ has the strongest influence on C_f. The influence of the roughness parameter E is about 7 times smaller whereas the distance d to the wall has a negligible effect, except near the leading edge. For example, using a linear Taylor series, a 5% increase in κ is expected to produce the 6% increase of C_f at $x/L = 0.8$. Thus, the influence of κ on C_f is even more pronounced than that of C_2. Finally, the negative sign of C_f' for the roughness parameter indicates that E should be reduced to increase the wall shear stress. As we see, sensitivities can contribute to our understanding of the model.

To validate the above estimated increases in C_2 (+9%) and κ (+5%) needed to achieve an increase of 6% in C_f at $x/L = 0.8$, we computed two new flow solutions: one at $C_2 = 2.09$ and the other at $\kappa = 0.44$. Figure 13 shows that the simulations at these perturbed values of the parameters succeed in recovering the Schultz-Grunow's correlation at $x/L = 0.8$. Moreover, the two solutions are almost identical over the entire length of the plate. However, the discrepancy between the predictions and the Schultz-Grunow correlation has only been halved at $x/L = 0.25$. Finally, it has been increased for $x/L < 0.1$.

The distance to the wall d is particularly interesting to study because its value is not well determined a priori and depends on a user's choice. Ideally, we want d to

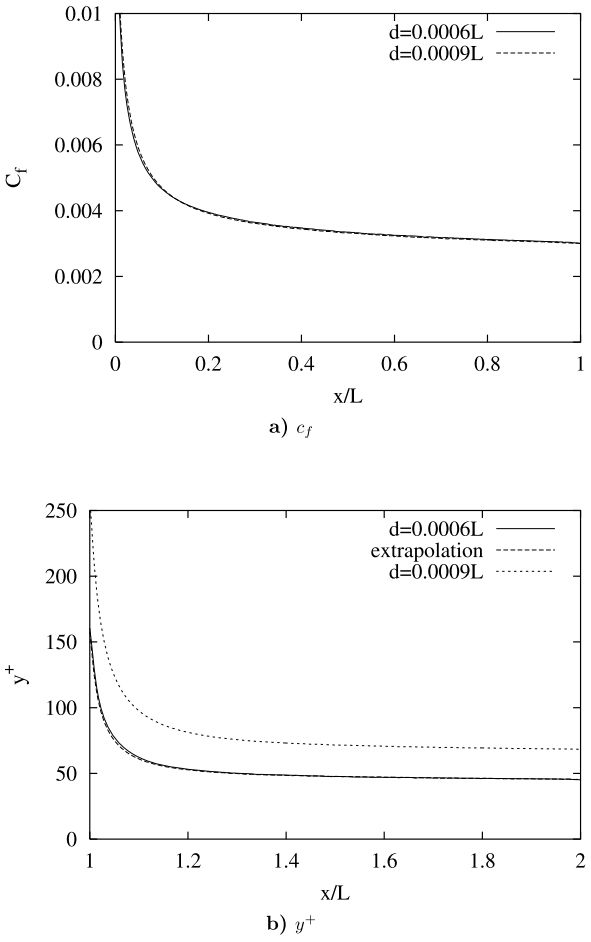

Fig. 14 Flat plate: effect of d on C_f and y^+

have little or no effect on the resulting predictions, in the sense that the wall function and turbulence model connect naturally and seamlessly, irrespective of the position of their interface. Figure 12 suggests that the choice of d is not crucial: C_f is virtually insensitive to d except near the leading edge. To verify this, we computed a new flow solution using $d = 0.0006L$, which corresponds to a large change (33% of the nominal valued of $d = 0.0009L$). As seen on Fig. 14(a), C_f is almost identical for these two different choices of d, validating the sensitivity computation. However, this conclusion does not generalize to all flows. For example, Lacasse et al. (2002) showed that, for a turnaround duct, separation may be predicted or not depending on the choice of d. In all cases, d should be chosen such that y^+ remains in a valid range. In particular, one should avoid y^+ going below 30. Sensitivities can be used to predict y^+ for nearby configurations and validate it prior to computing this new flow. In this example, $y^{+\prime}$ was examined before selecting $d = 0.006L$. Figure 14(b) shows the distribution of y^+ at $d = 0.0006L$, the linearly extrapolated solution using the sensitivities, and the recomputed solution at $d = 0.006$. As predicted by the extrapolation, y^+ remains within a valid range over the entire plate surface. Moreover,

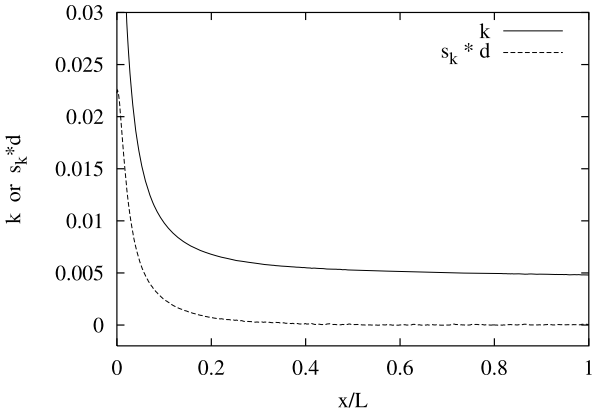

Fig. 15 Distribution of k and $\frac{\partial k}{\partial d}d$ on the flat plate

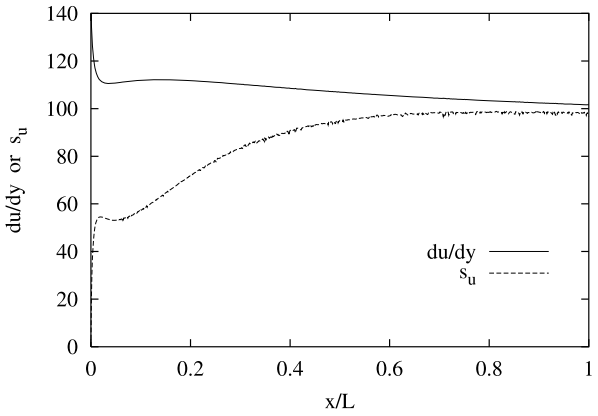

Fig. 16 Comparison of $\frac{\partial u}{\partial y}$ and $\frac{\partial u}{\partial d}$

the extrapolation is very accurate, indicating that y^+ is almost a linear function of d as one would infer from (11). Note that $y^{+\prime}$ may differ from zero under certain circumstances (see (18)).

According to the wall function, k should be constant through the boundary layer thickness (in the log-law region). Ideally, the boundary value of k should thus be insensitive to d. Figure 15 confirms this: on the rear part of the plate, the scaled sensitivity of k ($d\frac{\partial k}{\partial d}$ is much smaller than k itself and is close to zero).

Finally, if the turbulence model and the universal velocity profile used in the wall function were equivalent in the log-law region, then changing d while maintaining the geometry fixed would be equivalent to translating the geometry while keeping d fixed. For this perfect cohesion between the turbulence model and the wall function, we would have $s_u = \frac{\partial u}{\partial d}$ equal to $\frac{\partial u}{\partial y}$. Figure 16 compares s_u and $\frac{\partial u}{\partial y}$. Note that $\frac{\partial u}{\partial y}$ was recovered using the shear stress evaluated from the wall function,

$$\frac{\partial u}{\partial y} = \frac{\tau_w}{\mu + \mu_t}$$

because this is more accurate than the finite element derivative. Note that s_u is large even if C_f' is almost zero. The agreement is poor on the front half of the plate but good

on the rear half. Hence, the turbulence model and the wall function velocity profile are not in perfect agreement. This also indicates that the velocity profile, plotted against the distance to the real wall, is influenced by d even if C_f is not.

7 Conclusions

A general methodology was presented and applied to sensitivity analysis of turbulent flows. An adaptive finite element method was used to solve the differential equations for the flow and its sensitivities. The methodology delivers accurate results. The paper has demonstrated several uses of sensitivities other than optimal design. In particular, they may be used for:

- identification or ranking of key parameters controlling the flow,
- identification or ranking of parameters that have little effect on the flow,
- fast evaluation of solution for nearby values of the parameters (i.e. answer what if questions),
- uncertainty analysis.

The methodology was verified on a problem possessing a closed form solution solution (decay of grid turbulence). Sensitivity analysis of the backward facing step problem has shown that C_1 and C_2 have the most pronounced effect on the turbulence model predictions. Furthermore, the observed discrepancies between predictions and experimental measurements cannot be explained by small estimated data uncertainty on the closure coefficients.

For the flat plate problem, the skin friction coefficient is under-predicted by the k–ϵ turbulence model with wall functions. Sensitivity analysis indicates that the flow response is most sensitive to C_2 and κ. Their effect is pronounced enough that perturbations of less that 10% are sufficient to bring skin friction predictions up to the level of the Schultz-Grunow's correlation at $x/L = 0.8$. The parameters σ_k and d have very small effects. However, the velocity profile is influenced by d, indicating a lack of consistency between the wall function and the k–ϵ model.

Sensitivities can be used in a Taylor series expansion to compute nearby flows accurately and quickly. The accuracy of this approach was verified by comparing these inexpensive predictions with a full flow solution at the perturbed values of the parameters.

Acknowledgements This work was sponsored in part by the Canada Research Chair Program (Government of Canada), the National Science and Engineering Research Council (NSERC, Government of Canada), the Fond Québecois pour la Recherche sur la Nature et la Technologie (FQRNT, Government of Québec), and by the Air Force Office of Scientific Research under grant AFOSR F49620-00-1-0299.

References

Blackwell BF, Dowding KJ, Cochran RJ, Dobranich D (1998) Utilization of sensitivity coefficients to guide the design of a thermal battery. ASME IMECE 361:73–82

Borggaard J, Pelletier D (1998) Optimal shape design in forced convection using adaptive finite elements. In: 36th AIAA aerospace sciences meeting and exhibit, Reno, NV, January 1998. AIAA Paper 98-0908

Borggaard J, Pelletier D, Turgeon É (2000) A study of optimal cooling strategies in thermal processes. In: 38th AIAA aerospace sciences meeting and exhibit, Reno, NV, January 2000. AIAA Paper 2000-0563

Burden RL, Faires JD, Reynolds AC (1981) Numerical analysis, 2th edn. Prindle, Weber and Schmidt, Boston, p. 10

Chabard JP (1991) Projet N3S de mécanique des fluides—manuel théorique de la version 3. Tech. Rep. EDF HE-41/91.30B, Électricité de France

Craig KJ, Venter PJ (1999) Optimization of the k–ϵ coefficients for separation on a high-lift airfoil. In: 37th AIAA aerospace sciences meeting and exhibit, Reno, NV, January 1999. AIAA Paper 99-0151

Galera S, Hallo L, Puigt G, Mohammadi B (2005) Wall laws for heat transfer predictions in thermal turbulent flows. In: 38th AIAA thermophysics conference, Toronto, ON, Canada, June 2005. AIAA 2005-5200

Gerald CF, Wheatley PO (1998) Applied numerical analysis, 4th edn. Addison–Wesley, New York, p. 46

Godfrey AG, Cliff EM (2001) Sensitivity equations for turbulent flows. In: 39th AIAA aerospace sciences meeting and exhibit, Reno, NV, January 2001. AIAA Paper 2001-1060

Godfrey AG, Eppard WM, Cliff EM (1998) Using sensitivity quations for chemically reacting flows. In: 7th AIAA/USAF/NASA/ISSMO symposium on multidisciplinary analysis and optimization, St. Louis, Missouri, September 1998, pp. 789–798. AIAA Paper 98-4805

Gunzburger MD (1999) Sensitivities, adjoints, and flow optimization. Int J Numer Methods Fluids 31:53–78

Ignat L, Pelletier D, Ilinca F (1998) Adaptive computation of turbulent forced convection. Numer Heat Transf Part A 34:847–871

Ilinca F (1996) Méthodes d'éléments finis adaptatives pour les écoulements turbulents. PhD thesis, École Polytechnique de Montréal

Ilinca F, Pelletier D (1997) A Unified approach for adaptive solutions of compressible and incompressible flows. In: 35th AIAA aerospace sciences meeting and exhibit, Reno, NV, January 1997. AIAA Paper 97-0330

Ilinca F, Pelletier D (1998) Positivity preservation and adaptive solution for the k–ϵ model of turbulence. AIAA J 36(1):44–51

Ilinca F, Pelletier D, Garon A (1997a) An adaptive finite element method for a two-equation turbulence model in wall-bounded flows. Int J Numer Methods Fluids 24:101–120

Ilinca F, Pelletier D, Arnoux-Guisse F (1997b) An adaptive finite element scheme for turbulent free shear flows. Int J CFD 8:171–188

Ilinca F, Pelletier D, Ignat L (1998) Adaptive finite element solution of compressible turbulent flows. AIAA J 36(12):2187–2194

Kim JJ (1978) Investigation of separation and reattachment of turbulent shear layer: flow over a backward facing step. PhD thesis, Stanford University

Lacasse D, Turgeon É, Pelletier D (2001) On the judicious use of the k–ϵ model, wall functions and adaptivity. Int J Therm Sci 43:925–938

Lacasse D, Turgeon É, Pelletier D (2002) Predictions of turbulent separated flow in a turnaround duct using wall functions and adaptivity. Int J CFD 15:209–225

Launder BE, Spalding J (1974) The numerical computation of turbulent flows. Comput Methods Appl Mech Eng 3(2):269–289

Limache A, Cliff E (1999) Aerodynamic sensitivity theory for rotary stability derivatives. In: Proceedings of the AIAA atmospheric flight mechanics conference. AIAA Paper Number 99-4313

Pelletier D, Ilinca F (1997) Adaptive remeshing for the k–ϵ model of turbulence. AIAA J 35(4):640–646

Pelletier D, Turgeon E, Etienne S, Borggaard J (2002) Reliable sensitivity analysis by an adaptive sensitivity equation method. In: 3rd AIAA theoretical fluid mechanics conference, St. Louis, MO, June 2002. AIAA Paper 2002–2758

Peraire J, Vahdati M, Morgan K, Ziekiewicz O (1987) Adaptive remeshing for compressible flow computations. J Comput Phys 72(2):449–466

Ralston A, Abramowitz P (1981) A first course in numerical analysis, 2nd edn. MCGraw–Hill, New York, p. 5

Roache P (1998) Verification and validation in computational science and engineering. Hermosa, Albuquerque

Schlichting H (1979) Boundary-layer theory, 7th edn. McGraw–Hill, New York

Schultz-Grunow F (1941) New frictional resistance law for smooth plates. NACA TM 986

Turgeon É (1997) Application d'une méthode d'éléments finis adaptative à des écoulements axisymétriques. Master's thesis, École Polytechnique de Montréal

Turgeon, É, Pelletier D, Borggaard J (2000a) A general continuous sensitivity equation formulation for complex flows. In: 8th AIAA/NASA/USAF/ISSMO symposium on multidisciplinary analysis and optimization, Long Beach, CA, September 2000. AIAA Paper 2000-4732

Turgeon É, Pelletier D, Borggaard J (2000b) A continuous sensitivity equation method for flows with temperature dependent properties. In: 8th AIAA/NASA/USAF/ISSMO symposium on multidisciplinary analysis and optimization, Long Beach, CA, September 2000. AIAA Paper 2000-4821

Turgeon É, Pelletier D, Borggaard J (2000c) A continuous sensitivity equation approach to optimal design in mixed convection. Numer Heat Transf Part A 38:869–885

Turgeon É, Pelletier D, Borggaard J (2001a) A General continuous sensitivity equation formulation for the k–ϵ model of turbulence. In: 15th AIAA computational fluid dynamics conference, Anaheim, CA, June 2001. AIAA Paper 2001-3000

Turgeon É, Pelletier D, Borggaard J (2001b) Sensitivity and uncertainty analysis for variable property flows. In: 39th AIAA aerospace sciences meeting and exhibit, Reno, NV, January 2001. AIAA Paper 2001-0139

Turgeon E, Pelletier D, Borggaard J (2004) A general continuous sensitivity equation formulation for the k–ϵ model of turbulence. Int J CFD 1:29–46

White FM (1974) Viscous flow. McGraw–Hill, New York

Zienkiewicz OC, Zhu JZ (1992a) The superconvergent patch recovery and a posteriori error estimates, part 1: the recovery technique. Int J Numer Methods Eng 33:1331–1364

Zienkiewicz OC, Zhu JZ (1992b) The superconvergent patch recovery and a posteriori error estimates, part 2: error estimates and adaptivity. Int J Numer Methods Eng 33:1365–1382